An analytical spectral stiffness method for buckling of rectangular plates on Winkler foundation subject to general boundary conditions

Xiang Liu [a,b,c], Xiao Liu [a,b], Wei Zhou [a,b,*]

[a] Key Laboratory of Traffic Safety on Track, Ministry of Education, School of Traffic and Transportation Engineering, Central South University, China
[b] Joint International Research Laboratory of Key Technology for Rail Traffic Safety, Central South University, China
[c] State Key Laboratory of High Performance Complex Manufacturing, Central South University, China

ARTICLE INFO

ABSTRACT

An analytical spectral stiffness method is proposed for the efficient and accurate buckling analysis of rectangular plates on Winkler foundation subject to general boundary conditions (BCs). The method combines the advantages of superposition method, stiffness-based method and the Wittrick–Williams algorithm. First, exact general solutions of the governing differential equation (GDE) of plate buckling considering both elastic foundation and biaxial loading is derived by using a modified Fourier series. The superposition of such general solutions satisfy the GDE exactly and BCs approximately, which guarantees the rapid convergence and high accuracy. Then, based on the exact general solution, the spectral stiffness matrix which relates the coefficients of plate generalized displacement BCs and force BCs is symbolically developed. As a result, arbitrary BCs can be prescribed straightforwardly in the stiffness-based model. As an efficient and reliable solution technique, the Wittrick–Williams algorithm with the J_0 problem resolved is applied to obtain the critical buckling solutions. The accuracy and efficiency of the method are verified by comparing with other methods. Benchmark buckling solutions are provided for plates with all possible boundary conditions. Also, dependence of various factors such as foundation stiffness, load combinations and aspect ratio on the buckling behaviors are investigated.

© 2020 Elsevier Inc. All rights reserved.

1. Introduction

Plate structures have been used in mechanical engineering, aviation, and ship-building as they are light and strong. However, due to certain complex load combinations, structural instability can arise. Buckling is a common form of instability, manifest as either local, or global buckling. Global buckling instability will lead to a sudden change in geometry and the loss of bearing capacity, while local buckling instability will lead to the reduction of the effective section of some structures and the failure of some components which will accelerate the overall instability of the structure. Once buckling occurs in a plate, the structure loses its serviceability, which is far more dangerous than the loss of strength. This can also be confirmed by many practical engineering accidents. As for the cause of buckling instability of a plate, the load combination, boundary

conditions (BCs), and support condition all exert an important influence on the occurrence of buckling. Therefore, it is an important problem that needs to be solved when designing the structure of plates under various load combinations to ensure that buckling analysis is in accordance with arbitrary boundary and support conditions so as to avoid instability.

Numerical methods are frequently used in the buckling analysis of plates by engineers and researchers because they usually meet engineering requirements and the error is within an acceptable range. Methods in this category included, but not limited to, finite element [1], finite difference [2], boundary element [3], finite strip [4,5], differential quadrature [6] and its extensions [7,8], discrete singular convolution [9], generalized integral transformation [10] and etc. Although these numerical methods can easily cope with plate buckling considering general boundary conditions, these methods usually require a refined domain grid for more accurate results. In parametric or optimisation studies, remeshment is required, which often leads to unacceptable computational efficiency and accuracy. In this regard, analytical methods are ideal alternatives to provide efficient and accurate predictions for parametric and optimization studies.

It is well-known that analytical buckling solutions can be derived for Levy-type plates with as least one pair of opposite edges are simply supported [11–13]. The first contribution in this regard was probably made by Bryan [14], who proposed a buckling solution of isotropic rectangular plates, simply supported on four sides. Later, exact buckling solutions are proposed for simply supported plates under shear [15], uni-/bi-axial tension and/or compression with uniform [16–20] and non-uniform [21–24] distributions, those with variable thickness and elastic modulus [25] and stiffeners [26] and Levy plates on elastic foundation [27–29]. Also, an applicable buckling formula was proposed for plates subjected to both biaxial and shear loads [30]. More recently, exact Levy-type buckling solutions are obtained for Mindlin plates on elastic foundation [31], thick plate made of both isotropic [32] and functionally graded materials [33,34]. Based on the Levy-type solutions, exact stiffness method (or exact strip method) was firstly proposed by Wittrick and Williams [35] for buckling analysis of Levy-type plate structures. Further exact stiffness formulations are developed to investigate the critical buckling of curved composite plates [36], delaminated composite plates [37,38] and thick composite plates [39]. Although the above methods are limited to Levy-type plates, it is worthy highlighting that the exact stiffness method is stiffness-based which facilitates the assembly procedure as well as the application of various boundary conditions on the nodal edges very straightforwardly.

For buckling analysis of plates with more general boundary conditions, many researchers have made contributions by using different analytical methods, such as the Rayleigh-Ritz method [40,41], superposition method [42,43] and its extensions [44–50], Kantorovich-based methods [51–53] amongst many others [54–56]. The Rayleigh–Ritz method [40,41] is a very common and popular method since it is very versatile in modeling both governing differential equations (GDEs) and boundary conditions (BCs). In this method, the GDEs are satisfied approximately by chosen admissible functions and BCs are enforced by using penalty method [57] or Lagrangian multipliers. However, some drawbacks may be involved in some cases such as the need of choosing proper admissible functions and also inaccuracy or numerical instabilities may be introduced upon satisfaction of boundary and continuity conditions [58]. On the other hand, superposition method [42,43] is an efficient and accurate analytical method for eigenvalue analysis of plates where the GDE is satisfied exactly and BCs is satisfied approximately. Cleghorn and Yu [44] used the superposition method to develop the buckling solutions of the rectangular thin plates with complete fixed support and simple opposite support. Li and his co-authors [46–48] studied the buckling behaviors of rectangular plates under three types of BCs by using the symplectic superposition method. Papkov and Banerjee [45] has proposed a limitant theory combined with superposition method which can be applied to plate vibration and buckling analyses. Their method permits the evaluation of upper and low bounds at the same time, which is a significant advantage. Tenenbaum et al. [49,50] combined the superposition method with a stability determination method for solving the buckling loads of isotropic and orthotropic rectangular plates with different classical boundary conditions. Although the superposition-based methods exhibit high accuracy and rapid convergence rate, different formulae are needed for different BCs. Moreover, buckling eigenvalues are found by extensively evaluating the determinant (or inverse) of the analytical matrix [46,47] at a wide range of buckling load parameters, which is likely to miss some of the eigenvalues, increase the numerical cost significantly and involve some numerical instabilities in some cases. Some important properties of the above Rayleigh–Ritz method and superposition methods are given and compared in Table 1. Besides, Shufrin et al. [52] adopted a semi-analytical extended Kantorovich method [59] for buckling analysis of laminated rectangular plates under general BCs. By combining Kantorovich procedure and Galerkin method, Lopatin and Morozovb [53] derived the analytical buckling solutions of orthotropic rectangular plates with two opposite edges fixed and the other two free and subjected to linearly distributed in-plane loads. However, the results of Kantorovich-based method have discrepancy with accurate solutions due to the nature of the method as explained in [60]. Ruocco and his co-authors [54–56] discussed the buckling behaviors of composite plates under different BCs by using a semi-analytical method. In this type of method, the deformation in one direction is described by four pre-assumed functions which does not necessarily form a complete set, therefore introducing inaccuracy in the results.

It is clear from the above review that different analytical methods have different advantages and disadvantages on buckling analysis of plates. Is that possible to propose a highly efficient and accurate analytical method for buckling analysis of plates considering any arbitrary BCs and foundation supports, by combining those methods' advantages and meanwhile avoiding their disadvantages? A possibility has been opened up in recent years, that a new analytical method called the spectral dynamic stiffness method has been successfully developed for the free vibration analysis of plates structures [62–64] with general boundary conditions, which has been demonstrated to be a highly accurate and efficient method. Thus, the main objective of this paper is to extend the method to stability analysis by proposing a spectral stiffness formulation for buckling analysis of plates with general BCs on elastic foundation and developing related solution techniques. Firstly, the

Table 1

Comparisons on the properties of three different analytical methods for buckling analysis of rectangular plates with non-Levy-type boundary conditions.

|	Rayleigh–Ritz method	Superposition method	Present
Formulations (Shape functions, abbr. SFs)			
GDE (domain)	Approximate	Exact	Exact
BCs(boundary)	Approximate (Lagrangian multiplier or penalty method)	Approximate (series)	Approximate (series)
Convergence	Depend on how SFs satisfy GDE & BCs	Rapid	Rapid
Building blocks (BB)	Unique BB for general BCs	Different BB for different BCs	Unique BB for general BCs
Matrices	Symmetric stiffness & geometric stiffness	Nonsymmetric, could be stiffness/non-stiffness	Symmetric stiffness
Solution technique			
Solvers	Linear algebra solvers	Matrix determinant or inversion	Wittrick-Williams algorithm
Efficiency	Medium (due to large number of DOFs)	Medium (due to intensive determinant & inverse calculations)	High
Numerical stability	Depends on 2D SFs' orthogonality [61] & penalty parameter [57]	Might be unstable	Stable (due to 1D modified Fourier series' orthogonality)
Possible of missing roots	Impossible	Likely	Impossible
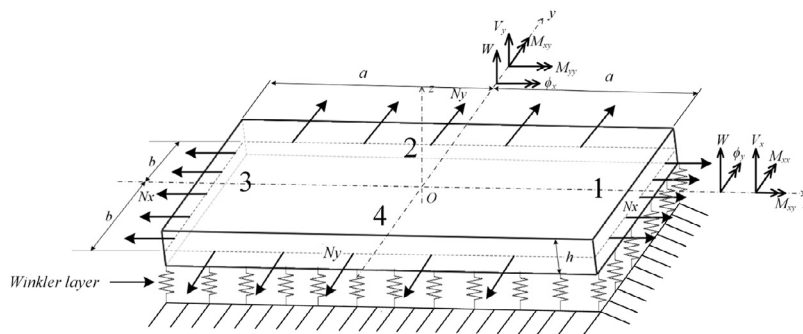
Fig. 1. Coordinate system and notations for a rectangular plate placed on elastic Winkler foundation.

exact general solution of the governing partial differential equation (GDE) for plate buckling considering foundation stiffness is derived by using the modified Fourier series (MFS). At the same time, the BCs of the generalized displacements and forces of the plates are expressed by the MFS. Then the spectral stiffness formulation is derived to correlate the MFS coefficients of all displacements and forces BCs. It is worth noting that the spectral stiffness formulation satisfies the GDE exactly and any arbitrary BCs can be prescribed straightforwardly by in the form of the MFS coefficients. Finally, the generalized Wittrick–Williams algorithm is used to solve the eigenvalue problem of the spectral stiffness matrix. The critical buckling solution of plate structure can be obtained efficiently and accurately. Essentially, the proposed method has the advantages of different methods (see Table 1), i.e., the rapid convergence rate and high accuracy of the superposition method [42], the easiness in describing general boundary conditions as in the stiffness-based method [35] and the high efficiency, numerical stability and certainty that no buckling mode will be missed by applying the Wittrick–Williams algorithm [65].

In the rest of this paper, the spectral stiffness formulation for rectangular plates on Winkler foundation is developed in Section 2. Then, Section 3 describes the solution technique, i.e., the generalized Wittrick–Williams algorithm for solving the corresponding buckling eigenproblem. Section 4 demonstrates its validity, accuracy and versatility, and investigates the effects of foundation stiffness, load combination and aspect ratio on the buckling behaviors, and where benchmark solutions are provided for plate buckling under all possible BCs. Finally, Section 5 concludes the paper.

2. Spectral stiffness formulation for a rectangular plate on Winkler foundation with general boundary conditions

2.1. Governing differential equation and general solutions

Fig. 1 shows an isotropic Kirchhoff plate with dimension $[-a, a] \times [-b, b]$ and thickness h and laid on an elastic Winkler foundation. The plate is subjected to inplane loading in the x ($\hat{N}_x$) and y ($\hat{N}_y$) directions, which could be either tensile(positive) and compressive(negative). The governing differential equation (GDE) for buckling of a thin plate placed on elastic Winkler foundation can be formulated based on variational principle [66] as follows

$$D\left[\frac{\partial^4 w}{\partial x^4} + 2\frac{\partial^4 w}{\partial x^2 \partial y^2} + \frac{\partial^4 w}{\partial y^4}\right] - \hat{N}_x \frac{\partial^2 w}{\partial x^2} - \hat{N}_y \frac{\partial^2 w}{\partial y^2} + \hat{k}w = 0, \tag{1}$$

where $(x, y) \in [-a, a] \times [-b, b]$, D is the bending stiffnesses and $\hat{k}$ is the stiffness of the Winkler foundation.

By dividing both sides of Eq. (1) by D, one may get

$$\frac{\partial^4 w}{\partial x^4} + 2 \frac{\partial^4 w}{\partial x^2 \partial y^2} + \frac{\partial^4 w}{\partial y^4} - N_x \frac{\partial^2 w}{\partial x^2} - N_y \frac{\partial^2 w}{\partial y^2} + kw = 0 \,, \tag{2}$$

where

$$k = \hat{k}/D \,, \quad N_x = \hat{N}_x/D \,, \quad N_y = \hat{N}_y/D \,.$$

The general solution for Eq. (2) is derived based on the variable separation principle following a similar procedure as the spectral dynamic stiffness method (SDSM) [60,67]. It has been proven mathematically and physically in [67] that for a rectangular element (2D), a two-series general solution should be sought which forms a complete set of the solutions for the rectanguler element with arbitrary boundary conditions (BCs)

$$w(x, y) = \sum_{m=1}^{\infty} X_m^*(x) \hat{Y}_m(y) + \sum_{n=1}^{\infty} Y_n^*(y) \hat{X}_n(x), \tag{3}$$

where $X_m^*(x)$ and $Y_n^*(y)$ described in $x \in [-a, a]$ and $y \in [-b, b]$ take the form of one-dimensional (1D) modified Fourier basis functions

$$X_m^*(x) = \mathcal{T}_k(\alpha_{km}x) = \begin{cases} \cos(\alpha_{km}x), & k = 0 \\ \sin(\alpha_{km}x), & k = 1 \end{cases} \tag{4a}$$

$$Y_n^*(y) = \mathcal{T}_j(\beta_{jn}y) = \begin{cases} \cos(\beta_{jn}y), & j = 0 \\ \sin(\beta_{jn}y), & j = 1 \end{cases} \tag{4b}$$

where $\mathcal{T}_k$, $\mathcal{T}_j$ represent modified Fourier basis functions with the wavenumbers α_{km} and β_{jn} which are shown as follows

$$\alpha_{km} = \begin{cases} m\pi/a & k = 0 \\ (m + 1/2)\pi/a & k = 1 \end{cases}, \qquad \beta_{jn} = \begin{cases} n\pi/b & j = 0 \\ (n + 1/2)\pi/b & j = 1 \end{cases}. \tag{5}$$

Consequently, a two-series general solution of GDE of Eq. (2) in the form of Eq. (3) can be derived

$$\begin{aligned} w(x, y) = & \sum_{\substack{m \in \mathbb{N} \\ k \in \{0,1\}}} \mathcal{T}_k(\alpha_{km}x) \Big[C_{km1} \mathrm{ch}(p_{1km}y) + C_{km2} \mathrm{ch}(p_{2km}y) + C_{km3} \mathrm{sh}(p_{1km}y) + C_{km4} \mathrm{sh}(p_{2km}y) \Big] \\ & + \sum_{\substack{n \in \mathbb{N} \\ j = \{0,1\}}} \mathcal{T}_j(\beta_{jn}y) \Big[C_{jn1} \mathrm{ch}(q_{1jn}x) + C_{jn2} \mathrm{ch}(q_{2jn}x) + C_{jn3} \mathrm{sh}(q_{1jn}x) + C_{jn4} \mathrm{sh}(q_{2jn}x) \Big], \end{aligned} \tag{6}$$

where the wave parameters p_{1km}, p_{2km} and q_{1jn}, q_{2jn} are obtained as follows. Substituting the $X_m^*(x)$ and $Y_n^*(y)$ of Eq. (4) into Eq. (2) leads to the following two characteristic equations, respectively.

$$\begin{cases} \alpha_{km}^4 - 2\alpha_{km}^2 p_{km}^2 + p_{km}^4 + N_x \alpha_{km}^2 - N_y p_{km}^2 + k = 0 \\ q_{jn}^4 - 2q_{jn}^2 \beta_{jn}^2 + \beta_{jn}^4 - N_x q_{jn}^2 + N_y \beta_{jn}^2 + k = 0 \end{cases}. \tag{7}$$

Therefore,

$$\begin{cases} p_{1,2km} = \sqrt{\dfrac{N_y}{2} + \alpha_{km}^2 \mp \sqrt{\dfrac{N_y^2}{4} + (N_y - N_x)\alpha_{km}^2 - k}} \\ q_{1,2jn} = \sqrt{\dfrac{N_x}{2} + \beta_{jn}^2 \mp \sqrt{\dfrac{N_x^2}{4} + (N_x - N_y)\beta_{jn}^2 - k}} \end{cases}. \tag{8}$$

Additionally, it should be noted in passing that, for any $k, j \in \{0, 1\}, m, n \in \mathbb{N}$, we can get the following relationships based on Eq. (8).

$$p_{1km}^2 + p_{2km}^2 = 2\alpha_{km}^2 + N_y \,, \quad p_{1km}^2 p_{2km}^2 = \alpha_{km}^4 + N_x \alpha_{km}^2 + k \,, \tag{9a}$$

$$q_{1jn}^2 + q_{2jn}^2 = 2\beta_{jn}^2 + N_x \,, \quad q_{1jn}^2 q_{2jn}^2 = \beta_{jn}^4 + N_y \beta_{jn}^2 + k \,, \tag{9b}$$

$$p_{2km}^2 - p_{1km}^2 = \sqrt{N_y^2 + 4(N_y - N_x)\alpha_{km}^2 - 4k}, \tag{9c}$$

$$q_{2jn}^2 - q_{1jn}^2 = \sqrt{N_x^2 + 4(N_x - N_y)\beta_{jn}^2 - 4k}, \tag{9d}$$

$$(p_{1km}^2 + \beta_{jn}^2)(p_{2km}^2 + \beta_{jn}^2) = (q_{1jn}^2 + \alpha_{km}^2)(q_{2jn}^2 + \alpha_{km}^2) = \alpha_{km}^4 + 2\alpha_{km}^2\beta_{jn}^2 + \beta_{jn}^4 + N_x\alpha_{km}^2 + N_y\beta_{jn}^2 + k. \tag{9e}$$

Next, by using the symmetric and anti-symmetric properties of trigonometric functions and hyperbolic functions, we can divide the general solution $w(x, y)$ of Eq. (6) into the sum of the four solution components.

$$w(x, y) = \sum_{k,j \in \{0,1\}} w^{kj}(x, y) = w^{00} + w^{01} + w^{10} + w^{11}, \tag{10}$$

where 'â0â for symmetric components and 'â1â for antisymmetric components respectively, k and j express the symmetry properties relating to x and y,

$$w^{kj}(x, y) = \sum_{m \in \mathbb{N}} \left\{ \sum_{i=1,2} \left[A_{ikm}\mathcal{H}_j(p_{ikm}y) \right] \mathcal{T}_k(\alpha_{km}x) \right\} + \sum_{n \in \mathbb{N}} \left\{ \sum_{i=1,2} \left[B_{ijn}\mathcal{H}_k(q_{ijn}x) \right] \mathcal{T}_j(\beta_{jn}y) \right\}, \tag{11}$$

and where A_{1km}, A_{2km}, B_{1jn} and B_{2jn} are unknown coefficients to be solved. $\mathcal{H}$ represents hyperbolic functions defined as follows.

$$\mathcal{H}_j(p_{ikm}y) = \begin{cases} \text{ch}(p_{ikm}y) & j = 0 \\ \text{sh}(p_{ikm}y) & j = 1 \end{cases}, \quad \mathcal{H}_k(q_{ijn}x) = \begin{cases} \text{ch}(q_{ijn}x) & k = 0 \\ \text{sh}(q_{ijn}x) & k = 1 \end{cases}. \tag{12}$$

Understandably, the kj solution components can be represented by the function only in the first quadrant ($x \times y = [0, a] \times [0, b]$).

2.2. Boundary conditions and spectral stiffness formulation

The boundary conditions (BCs) of the plate can be derived from the variational principle [66] to obtain Eq. (13)

$$\delta w; \quad v_x = -D\left[\frac{\partial^3 w}{\partial x^3} + (2 - \nu)\frac{\partial^3 w}{\partial x \partial y^2} - N_x \frac{\partial w}{\partial x} \right], \tag{13a}$$

$$\delta \phi_x = -\delta \frac{\partial w}{\partial x}; \quad m_{xx} = -D\left(\frac{\partial^2 w}{\partial x^2} + \nu \frac{\partial^2 w}{\partial y^2} \right), \tag{13b}$$

$$\delta w; \quad v_y = -D\left[\frac{\partial^3 w}{\partial y^3} + (2 - \nu)\frac{\partial^3 w}{\partial y \partial x^2} - N_y \frac{\partial w}{\partial y} \right], \tag{13c}$$

$$\delta \phi_y = -\delta \frac{\partial w}{\partial y}; \quad m_{yy} = -D\left(\frac{\partial^2 w}{\partial y^2} + \nu \frac{\partial^2 w}{\partial x^2} \right). \tag{13d}$$

In above equation ϕ_x and ϕ_y are the bending rotations, m_{xx}, m_{yy} are bending moments, v_x, v_y are shear forces, and ν is the Poisson ratio. It is noteworthy that buckling load coefficients N_x and N_y appear in the shear force BCs of Eqs. (13), which were derived from variational principle [66]. Some existing research for buckling analysis has taken wrong expressions [68] for force BCs as pointed out by Coman and Liu [69]. It is found that if problematic BCs are adopted in the spectral stiffness formulation, the developed stiffness matrix will not be symmetric as it should be. This is expected since problematic BCs violate the energy conservation law of the system physically and will lead to an asymmetric stiffness matrix from a mathematical point of view. Therefore, it is suggested to utilize the energy-based variational principle [66] which can help us avoid mistakes in derivation of GDEs and BCs.

Next, the above generalized displacement and force BCs will be adopted to develop the spectral stiffness formulation. In the above section, four kj solution components $w^{kj}(x, y)$ in the first quadrant of xOy plane, namely, $[0, a] \times [0, b]$ are representable. Accordingly, there are four kj components for the corresponding BCs, which can be expressed in terms of the modified Fourier series

$$
\begin{bmatrix} w_a^{kj} \\ w_b^{kj} \\ \phi_a^{kj} \\ \phi_b^{kj} \end{bmatrix} = \begin{bmatrix} \sum_{n \in \mathbb{N}} w_{ajn} \dfrac{\mathcal{T}_j(\beta_{jn}y)}{\sqrt{\zeta_{jn}b}} \\ \sum_{m \in \mathbb{N}} w_{bkm} \dfrac{\mathcal{T}_k(\alpha_{km}x)}{\sqrt{\zeta_{km}a}} \\ \sum_{n \in \mathbb{N}} \phi_{ajn} \dfrac{\mathcal{T}_j(\beta_{jn}y)}{\sqrt{\zeta_{jn}b}} \\ \sum_{m \in \mathbb{N}} \phi_{bkm} \dfrac{\mathcal{T}_k(\alpha_{km}x)}{\sqrt{\zeta_{km}a}} \end{bmatrix}, \quad \begin{bmatrix} v_a^{kj} \\ v_b^{kj} \\ m_a^{kj} \\ m_b^{kj} \end{bmatrix} = D \begin{bmatrix} \sum_{n \in \mathbb{N}} v_{ajn} \dfrac{\mathcal{T}_j(\beta_{jn}y)}{\sqrt{\zeta_{jn}b}} \\ \sum_{m \in \mathbb{N}} v_{bkm} \dfrac{\mathcal{T}_k(\alpha_{km}x)}{\sqrt{\zeta_{km}a}} \\ \sum_{n \in \mathbb{N}} m_{ajn} \dfrac{\mathcal{T}_j(\beta_{jn}y)}{\sqrt{\zeta_{jn}b}} \\ \sum_{m \in \mathbb{N}} m_{bkm} \dfrac{\mathcal{T}_k(\alpha_{km}x)}{\sqrt{\zeta_{km}a}} \end{bmatrix}, \tag{14}
$$

where $\sqrt{\zeta_{jn}b}$ and $\sqrt{\zeta_{km}a}$ were introduced [67] to ensure that the resultant component matrix $\boldsymbol{K}^{kj}$ remain symmetric for the general case when $a \neq b$.

Similar to the spectral dynamic stiffness method [60,67], the modified Fourier series coefficients for the kj components of both force and displacement BCs can be related by the spectral stiffness method. This is achieved by substituting the kj solution components of Eq. (11) into the natural BCs of Eq. (13).

$$
\begin{bmatrix} w_a^{kj} \\ w_b^{kj} \\ \phi_a^{kj} \\ \phi_b^{kj} \end{bmatrix} = \begin{bmatrix} w^{kj}|_{x=a} \\ w^{kj}|_{y=b} \\ -\partial_x w^{kj}|_{x=a} \\ -\partial_y w^{kj}|_{y=b} \end{bmatrix}, \quad \begin{bmatrix} v_a^{kj} \\ v_b^{kj} \\ m_a^{kj} \\ m_b^{kj} \end{bmatrix} = D \begin{bmatrix} -\left(\partial_x^3 + (2-\nu)\partial_x\partial_y^2 - N_x\partial_x\right)w^{kj}|_{x=a} \\ -\left(\partial_y^3 + (2-\nu)\partial_y\partial_x^2 - N_y\partial_y\right)w^{kj}|_{y=b} \\ -\left(\partial_x^2 + \nu\partial_y^2\right)w^{kj}|_{x=a} \\ -\left(\partial_y^2 + \nu\partial_x^2\right)w^{kj}|_{y=b} \end{bmatrix}. \tag{15}
$$

With the help of the expressions ϕ_a^{kj}, ϕ_b^{kj}, v_a^{kj} and v_b^{kj} of both Eqs. (14) and (15),

$$
- \partial_x w^{kj}\big|_{x=a} = \sum_{n \in \mathbb{N}} \phi_{ajn} \mathcal{T}_j(\beta_{jn}y) / \sqrt{\zeta_{jn}b}, \tag{16a}
$$

$$
- (\partial_x^3 + (2-\nu)\partial_x\partial_y^2 - N_x\partial_x)w^{kj}\big|_{x=a} = \sum_{n \in \mathbb{N}} v_{ajn} \mathcal{T}_j(\beta_{jn}y) / \sqrt{\zeta_{jn}b}, \tag{16b}
$$

$$
- \partial_y w^{kj}\big|_{y=b} = \sum_{m \in \mathbb{N}} \phi_{bkm} \mathcal{T}_k(\alpha_{km}x) / \sqrt{\zeta_{km}a}, \tag{16c}
$$

$$
- (\partial_y^3 + (2-\nu)\partial_y\partial_x^2 - N_y\partial_y)w^{kj}\big|_{y=b} = \sum_{m \in \mathbb{N}} v_{bkm} \mathcal{T}_k(\alpha_{km}x) / \sqrt{\zeta_{km}a}, \tag{16d}
$$

which yield

$$
- \phi_{ajn}/\sqrt{\zeta_{jn}b} = q_{1jn}\mathcal{H}_k^*(q_{1jn}a)B_{1jn} + q_{2jn}\mathcal{H}_k^*(q_{2jn}a)B_{2jn}, \tag{17a}
$$

$$
- v_{ajn}/\sqrt{\zeta_{jn}b} = \left(q_{1jn}^2 - (2-\nu)\beta_{jn}^2 - N_x\right)q_{1jn}\mathcal{H}_k^*(q_{1jn}a)B_{1jn} + \left(q_{2jn}^2 - (2-\nu)\beta_{jn}^2 - N_x\right)q_{2jn}\mathcal{H}_k^*(q_{2jn}a)B_{2jn}, \tag{17b}
$$

$$
- \phi_{bkm}/\sqrt{\zeta_{km}a} = p_{1km}\mathcal{H}_j^*(p_{1km}b)A_{1km} + p_{2km}\mathcal{H}_j^*(p_{2km}b)A_{2km}, \tag{17c}
$$

$$- v_{bkm}/\sqrt{\zeta_{km}}a = \left(p_{1km}^2 - (2-v)\alpha_{km}^2 - N_y\right)p_{1km}\mathcal{H}_j^*(p_{1km}b)A_{1km} + \left(p_{2km}^2 - (2-v)\alpha_{km}^2 - N_y\right)p_{2km}\mathcal{H}_j^*(p_{2km}b)A_{2km}.$$

(17d)

All unknown coefficients A_{1km}, A_{2km}, B_{1jn} and B_{2jn} of the general solution in Eq. (11) can be determined to be

$$B_{1jn} = \frac{v_{ajn} - (v\beta_{jn}^2 - q_{1jn}^2)\phi_{ajn}}{\sqrt{\zeta_{jn}}bq_{1jn}\mathcal{H}_k^*(q_{1jn}a)(q_{2jn}^2 - q_{1jn}^2)},$$

(18a)

$$B_{2jn} = -\frac{v_{ajn} - \left(v\beta_{jn}^2 - q_{2jn}^2\right)\phi_{ajn}}{\sqrt{\zeta_{jn}}bq_{2jn}\mathcal{H}_k^*\left(q_{2jn}a\right)\left(q_{2jn}^2 - q_{1jn}^2\right)},$$

(18b)

$$A_{1km} = \frac{v_{bkm} - (v\alpha_{km}^2 - p_{1km}^2)\phi_{bkm}}{\sqrt{\zeta_{km}}ap_{1km}\mathcal{H}_j^*(p_{1km}b)(p_{2km}^2 - p_{1km}^2)},$$

(18c)

$$A_{2km} = -\frac{v_{bkm} - \left(v\alpha_{km}^2 - p_{2km}^2\right)\phi_{bkm}}{\sqrt{\zeta_{km}}ap_{2km}\mathcal{H}_j^*(p_{2km}b)\left(p_{2km}^2 - p_{1km}^2\right)}.$$

(18d)

The above unknown coefficients are then substituted into the expressions for w_a^{kj}, w_b^{kj}, m_a^{kj} and m_b^{kj} in Eq. (14). Through a similar procedure as in [67], the modified Fourier series coefficients for all displacements and forces BCs can be related by the following matrix form

$$\begin{bmatrix} \boldsymbol{w}^{kj} \\ \boldsymbol{m}^{kj} \end{bmatrix} = \begin{bmatrix} \boldsymbol{A}_{w\phi}^{kj} & \boldsymbol{A}_{wv}^{kj} \\ \boldsymbol{A}_{m\phi}^{kj} & \boldsymbol{A}_{mv}^{kj} \end{bmatrix} \begin{bmatrix} \boldsymbol{\phi}^{kj} \\ \boldsymbol{v}^{kj} \end{bmatrix},$$

(19)

where

$$\boldsymbol{v}^{kj} = \begin{bmatrix} \boldsymbol{v}_a^{kj} \\ \boldsymbol{v}_b^{kj} \end{bmatrix}, \quad \boldsymbol{m}^{kj} = \begin{bmatrix} \boldsymbol{m}_a^{kj} \\ \boldsymbol{m}_b^{kj} \end{bmatrix}, \quad \boldsymbol{w}^{kj} = \begin{bmatrix} \boldsymbol{w}_a^{kj} \\ \boldsymbol{w}_b^{kj} \end{bmatrix}, \quad \boldsymbol{\phi}^{kj} = \begin{bmatrix} \boldsymbol{\phi}_a^{kj} \\ \boldsymbol{\phi}_b^{kj} \end{bmatrix}$$

(20)

and in which

$$\boldsymbol{v}_a^{kj} = [v_{aj0}, v_{aj1}, \cdots, v_{ajn}, \cdots]^T, \qquad\qquad \boldsymbol{v}_b^{kj} = [v_{bk0}, v_{bk1}, \cdots, v_{bkm}, \cdots]^T,$$
$$\boldsymbol{m}_a^{kj} = [m_{aj0}, m_{aj1}, \cdots, m_{ajn}, \cdots]^T, \qquad\qquad \boldsymbol{m}_b^{kj} = [m_{bk0}, m_{bk1}, \cdots, m_{bkm}, \cdots]^T,$$
$$\boldsymbol{w}_a^{kj} = [w_{aj0}, w_{aj1}, \cdots, w_{ajn}, \cdots]^T, \qquad\qquad \boldsymbol{w}_b^{kj} = [w_{bk0}, w_{bk1}, \cdots, w_{bkm}, \cdots]^T,$$
$$\boldsymbol{\phi}_a^{kj} = [\phi_{aj0}, \phi_{aj1}, \cdots, \phi_{ajn}, \cdots]^T, \qquad\qquad \boldsymbol{\phi}_b^{kj} = [\phi_{bk0}, \phi_{bk1}, \cdots, \phi_{bkm}, \cdots]^T.$$

The expressions for the four matrices $\boldsymbol{A}_{wv}^{kj}$, $\boldsymbol{A}_{m\phi}^{kj}$, $\boldsymbol{A}_{w\phi}^{kj}$ and $\boldsymbol{A}_{mv}^{kj}$ are given as follows

$$\boldsymbol{A}_{w\phi}^{kj}(n, n) = -(\Delta_1\Lambda_1 - \Delta_2\Lambda_2)/\Delta_5, \qquad\qquad \boldsymbol{A}_{w\phi}^{kj}(n, m) = -\Delta_7\Delta_9,$$
$$\boldsymbol{A}_{w\phi}^{kj}(m, n) = -\Delta_8\Delta_{10}, \qquad\qquad \boldsymbol{A}_{w\phi}^{kj}(m, m) = -(\Delta_3\Lambda_3 - \Delta_4\Lambda_4)/\Delta_6,$$
$$\boldsymbol{A}_{wv}^{kj}(n, n) = (\Lambda_1 - \Lambda_2)/\Delta_5, \qquad\qquad \boldsymbol{A}_{wv}^{kj}(n, m) = \Delta_7,$$
$$\boldsymbol{A}_{wv}^{kj}(m, n) = \Delta_8, \qquad\qquad \boldsymbol{A}_{wv}^{kj}(m, m) = (\Lambda_3 - \Lambda_4)/\Delta_6,$$
$$\boldsymbol{A}_{m\phi}^{kj}(n, n) = -\left(\Delta_1^2\Lambda_1 - \Delta_2^2\Lambda_2\right)/\Delta_5, \qquad\qquad \boldsymbol{A}_{m\phi}^{kj}(n, m) = -\Delta_7\Delta_{11},$$
$$\boldsymbol{A}_{m\phi}^{kj}(m, n) = -\Delta_8\Delta_{11}, \qquad\qquad \boldsymbol{A}_{m\phi}^{kj}(m, m) = -\left(\Delta_3^2\Lambda_3 - \Delta_4^2\Lambda_4\right)/\Delta_6,$$
$$\boldsymbol{A}_{mv}^{kj}(n, n) = (\Delta_1\Lambda_1 - \Delta_2\Lambda_2)/\Delta_5, \qquad\qquad \boldsymbol{A}_{mv}^{kj}(n, m) = \Delta_7\Delta_{10},$$
$$\boldsymbol{A}_{mv}^{kj}(m, n) = \Delta_8\Delta_9, \qquad\qquad \boldsymbol{A}_{mv}^{kj}(m, m) = (\Delta_3\Lambda_3 - \Delta_4\Lambda_4)/\Delta_6,$$

where

$$\Lambda_1 = \mathcal{TH}_k(q_{1jn}a)/q_{1jn}, \qquad\qquad \Lambda_2 = \mathcal{TH}_k(q_{2jn}a)/q_{2jn},$$

$$\Lambda_3 = \mathcal{TH}_j(p_{1km}b)/p_{1km}, \qquad\qquad \Lambda_4 = \mathcal{TH}_j(p_{2km}b)/p_{2km},$$

$$\Delta_1 = \nu\beta_{jn}^2 - q_{1jn}^2, \qquad\qquad \Delta_2 = \nu\beta_{jn}^2 - q_{2jn}^2,$$

$$\Delta_3 = \nu\alpha_{km}^2 - p_{1km}^2, \qquad\qquad \Delta_4 = \nu\alpha_{km}^2 - p_{2km}^2,$$

$$\Delta_5 = q_{2jn}^2 - q_{1jn}^2, \qquad\qquad \Delta_6 = p_{2km}^2 - p_{1km}^2,$$

$$\Delta_7 = 2(-1)^{m+n}/\left[\sqrt{\zeta_{km}\zeta_{jn}ab}\left(p_{1km}^2 + \beta_{jn}^2\right)\left(p_{2km}^2 + \beta_{jn}^2\right)\right],$$

$$\Delta_8 = 2(-1)^{m+n}/\left[\sqrt{\zeta_{km}\zeta_{jn}ab}\left(q_{1jn}^2 + \alpha_{km}^2\right)\left(q_{2jn}^2 + \alpha_{km}^2\right)\right],$$

$$\Delta_9 = \nu\alpha_{km}^2 + \beta_{jn}^2, \qquad\qquad \Delta_{10} = \alpha_{km}^2 + \nu\beta_{jn}^2,$$

$$\Delta_{11} = \alpha_{km}^2\beta_{jn}^2(1-\nu)^2 - \nu(\alpha_m^2 N_x + \beta_n^2 N_y + k),$$

$$\Delta_7 = \Delta_8 = 2(-1)^{m+n}/\left\{\sqrt{\zeta_{km}\zeta_{jn}ab}[(\alpha_{km}^2 + \beta_{jn}^2)^2 + N_x\alpha_{km}^2 + N_y\beta_{jn}^2 + k]\right\}.$$

It can be found that $\boldsymbol{A}_{wv}^{kj}$ and $\boldsymbol{A}_{m\phi}^{kj}$ are symmetric matrices and $\boldsymbol{A}_{w\phi}^{kj} = -\boldsymbol{A}_{mv}^{kj}{}^T$. This is because the formulation is a conservative system and we have also introduced $\sqrt{\zeta_{jn}b}$ and $\sqrt{\zeta_{km}a}$ in the modified Fourier series. Otherwise, these matrices will not have the above symplectic properties. By organizing coefficient vectors for force BCs on the left-hand side and displacement BCs on the right-hand side, we have

$$\boldsymbol{f}^{kj} = \boldsymbol{K}^{kj}\boldsymbol{d}^{kj}, \tag{21}$$

where

$$\boldsymbol{f}^{kj} = D\begin{bmatrix}\boldsymbol{v}^{kj}\\ \boldsymbol{m}^{kj}\end{bmatrix}, \quad \boldsymbol{d}^{kj} = \begin{bmatrix}\boldsymbol{w}^{kj}\\ \boldsymbol{\phi}^{kj}\end{bmatrix},$$

$$\boldsymbol{K}^{kj} = D\begin{bmatrix}\boldsymbol{A}_{wv}^{kj}{}^{-1} & -\boldsymbol{A}_{wv}^{kj}{}^{-1}\boldsymbol{A}_{w\phi}^{kj}\\ \boldsymbol{A}_{mv}^{kj}\boldsymbol{A}_{wv}^{kj}{}^{-1} & \boldsymbol{A}_{m\phi}^{kj} - \boldsymbol{A}_{mv}^{kj}\boldsymbol{A}_{wv}^{kj}{}^{-1}\boldsymbol{A}_{w\phi}^{kj}\end{bmatrix}.$$

Next, we need to develop the spectral stiffness matrix for a whole plate which relates the modified Fourier series coefficients of displacement BCs and force BCs. The displacement and force BCs on the four edges (denoted by subscripts 1, 2, 3 and 4 as in Fig. 1) of the plate can be written in the following vector form

$$\begin{bmatrix}w_1\\ \phi_1\\ w_2\\ \phi_2\\ w_3\\ \phi_3\\ w_4\\ \phi_4\end{bmatrix} = \begin{bmatrix}w(a,y)\\ \phi_x(a,y)\\ w(x,b)\\ \phi_y(x,b)\\ w(-a,y)\\ \phi_x(-a,y)\\ w(x,-b)\\ \phi_y(x,-b)\end{bmatrix}, \quad \begin{bmatrix}v_1\\ m_1\\ v_2\\ m_2\\ v_3\\ m_3\\ v_4\\ m_4\end{bmatrix} = \begin{bmatrix}v_x(a,y)\\ m_{xx}(a,y)\\ v_y(x,b)\\ m_{yy}(x,b)\\ v_x(-a,y)\\ m_{xx}(-a,y)\\ v_y(x,-b)\\ m_{yy}(x,-b)\end{bmatrix}. \tag{22}$$

Similar to Eq. (14), arbitrarily prescribed BCs on the four plate boundaries can be transformed into the vector form $\boldsymbol{f}$ and $\boldsymbol{d}$ by using the modified Fourier series formula. Since the general solution has been partitioned into four kj components as in Eq. (10), so the vectors $\boldsymbol{f}$, $\boldsymbol{d}$ for displacement and force BCs can be related to the four kj components $\boldsymbol{f}^{kj}$, $\boldsymbol{d}^{kj}$ of Eq. (21) with the relationship

$$\boldsymbol{f} = \begin{bmatrix}\boldsymbol{f}_1\\ \boldsymbol{f}_2\\ \boldsymbol{f}_3\\ \boldsymbol{f}_4\end{bmatrix} = \boldsymbol{T}\begin{bmatrix}\boldsymbol{f}^{00}\\ \boldsymbol{f}^{01}\\ \boldsymbol{f}^{10}\\ \boldsymbol{f}^{11}\end{bmatrix}, \quad \boldsymbol{d} = \begin{bmatrix}\boldsymbol{d}_1\\ \boldsymbol{d}_2\\ \boldsymbol{d}_3\\ \boldsymbol{d}_4\end{bmatrix} = \boldsymbol{T}\begin{bmatrix}\boldsymbol{d}^{00}\\ \boldsymbol{d}^{01}\\ \boldsymbol{d}^{10}\\ \boldsymbol{d}^{11}\end{bmatrix}, \tag{23}$$

in which

$$\boldsymbol{f}_i = \left[\boldsymbol{v}_i^{0^T}, \boldsymbol{v}_i^{1^T}, \boldsymbol{m}_i^{0^T}, \boldsymbol{m}_i^{1^T}\right]^T, \quad \boldsymbol{d}_i = \left[\boldsymbol{w}_i^{0^T}, \boldsymbol{w}_i^{1^T}, \boldsymbol{\phi}_i^{0^T}, \boldsymbol{\phi}_i^{1^T}\right]^T,$$ (24)

where $\boldsymbol{T}$ is the total transfer matrix taking the form

$$\boldsymbol{T} = \begin{bmatrix}
\boldsymbol{I}_n & \boldsymbol{O} & \boldsymbol{O} & \boldsymbol{O} & \boldsymbol{O} & \boldsymbol{O} & \boldsymbol{O} & \boldsymbol{O} & \boldsymbol{I}_n & \boldsymbol{O} & \boldsymbol{O} & \boldsymbol{O} & \boldsymbol{O} & \boldsymbol{O} & \boldsymbol{O} & \boldsymbol{O} \\
\boldsymbol{O} & \boldsymbol{O} & \boldsymbol{O} & \boldsymbol{O} & \boldsymbol{I}_n & \boldsymbol{O} & \boldsymbol{O} & \boldsymbol{O} & \boldsymbol{O} & \boldsymbol{O} & \boldsymbol{O} & \boldsymbol{O} & \boldsymbol{I}_n & \boldsymbol{O} & \boldsymbol{O} & \boldsymbol{O} \\
\boldsymbol{O} & \boldsymbol{I}_n & \boldsymbol{O} & \boldsymbol{O} & \boldsymbol{O} & \boldsymbol{O} & \boldsymbol{O} & \boldsymbol{O} & \boldsymbol{O} & \boldsymbol{I}_n & \boldsymbol{O} & \boldsymbol{O} & \boldsymbol{O} & \boldsymbol{O} & \boldsymbol{O} & \boldsymbol{O} \\
\boldsymbol{O} & \boldsymbol{O} & \boldsymbol{O} & \boldsymbol{O} & \boldsymbol{O} & \boldsymbol{I}_n & \boldsymbol{O} & \boldsymbol{O} & \boldsymbol{O} & \boldsymbol{O} & \boldsymbol{O} & \boldsymbol{O} & \boldsymbol{O} & \boldsymbol{I}_n & \boldsymbol{O} & \boldsymbol{O} \\
\boldsymbol{O} & \boldsymbol{O} & \boldsymbol{I}_m & \boldsymbol{O} & \boldsymbol{O} & \boldsymbol{O} & \boldsymbol{I}_m & \boldsymbol{O} & \boldsymbol{O} & \boldsymbol{O} & \boldsymbol{O} & \boldsymbol{O} & \boldsymbol{O} & \boldsymbol{O} & \boldsymbol{O} & \boldsymbol{O} \\
\boldsymbol{O} & \boldsymbol{O} & \boldsymbol{O} & \boldsymbol{O} & \boldsymbol{O} & \boldsymbol{O} & \boldsymbol{O} & \boldsymbol{O} & \boldsymbol{O} & \boldsymbol{O} & \boldsymbol{I}_m & \boldsymbol{O} & \boldsymbol{O} & \boldsymbol{O} & \boldsymbol{I}_m & \boldsymbol{O} \\
\boldsymbol{O} & \boldsymbol{O} & \boldsymbol{O} & \boldsymbol{I}_m & \boldsymbol{O} & \boldsymbol{O} & \boldsymbol{O} & \boldsymbol{I}_m & \boldsymbol{O} & \boldsymbol{O} & \boldsymbol{O} & \boldsymbol{O} & \boldsymbol{O} & \boldsymbol{O} & \boldsymbol{O} & \boldsymbol{O} \\
\boldsymbol{O} & \boldsymbol{O} & \boldsymbol{O} & \boldsymbol{O} & \boldsymbol{O} & \boldsymbol{O} & \boldsymbol{O} & \boldsymbol{O} & \boldsymbol{O} & \boldsymbol{O} & \boldsymbol{O} & \boldsymbol{I}_m & \boldsymbol{O} & \boldsymbol{O} & \boldsymbol{O} & \boldsymbol{I}_m \\
\boldsymbol{I}_n & \boldsymbol{O} & \boldsymbol{O} & \boldsymbol{O} & \boldsymbol{O} & \boldsymbol{O} & \boldsymbol{O} & \boldsymbol{O} & -\boldsymbol{I}_n & \boldsymbol{O} & \boldsymbol{O} & \boldsymbol{O} & \boldsymbol{O} & \boldsymbol{O} & \boldsymbol{O} & \boldsymbol{O} \\
\boldsymbol{O} & \boldsymbol{O} & \boldsymbol{O} & \boldsymbol{O} & \boldsymbol{I}_n & \boldsymbol{O} & \boldsymbol{O} & \boldsymbol{O} & \boldsymbol{O} & \boldsymbol{O} & \boldsymbol{O} & \boldsymbol{O} & -\boldsymbol{I}_n & \boldsymbol{O} & \boldsymbol{O} & \boldsymbol{O} \\
\boldsymbol{O} & -\boldsymbol{I}_n & \boldsymbol{O} & \boldsymbol{O} & \boldsymbol{O} & \boldsymbol{O} & \boldsymbol{O} & \boldsymbol{O} & \boldsymbol{O} & \boldsymbol{I}_n & \boldsymbol{O} & \boldsymbol{O} & \boldsymbol{O} & \boldsymbol{O} & \boldsymbol{O} & \boldsymbol{O} \\
\boldsymbol{O} & \boldsymbol{O} & \boldsymbol{O} & \boldsymbol{O} & \boldsymbol{O} & \boldsymbol{O} & -\boldsymbol{I}_n & \boldsymbol{O} & \boldsymbol{O} & \boldsymbol{O} & \boldsymbol{O} & \boldsymbol{O} & \boldsymbol{O} & \boldsymbol{I}_n & \boldsymbol{O} & \boldsymbol{O} \\
\boldsymbol{O} & \boldsymbol{O} & \boldsymbol{I}_m & \boldsymbol{O} & \boldsymbol{O} & \boldsymbol{O} & -\boldsymbol{I}_m & \boldsymbol{O} & \boldsymbol{O} & \boldsymbol{O} & \boldsymbol{O} & \boldsymbol{O} & \boldsymbol{O} & \boldsymbol{O} & \boldsymbol{O} & \boldsymbol{O} \\
\boldsymbol{O} & \boldsymbol{O} & \boldsymbol{O} & \boldsymbol{O} & \boldsymbol{O} & \boldsymbol{O} & \boldsymbol{O} & \boldsymbol{O} & \boldsymbol{O} & \boldsymbol{O} & \boldsymbol{I}_m & \boldsymbol{O} & \boldsymbol{O} & \boldsymbol{O} & -\boldsymbol{I}_m & \boldsymbol{O} \\
\boldsymbol{O} & \boldsymbol{O} & \boldsymbol{O} & -\boldsymbol{I}_m & \boldsymbol{O} & \boldsymbol{O} & \boldsymbol{O} & \boldsymbol{I}_m & \boldsymbol{O} & \boldsymbol{O} & \boldsymbol{O} & \boldsymbol{O} & \boldsymbol{O} & \boldsymbol{O} & \boldsymbol{O} & \boldsymbol{O} \\
\boldsymbol{O} & \boldsymbol{O} & \boldsymbol{O} & \boldsymbol{O} & \boldsymbol{O} & \boldsymbol{O} & \boldsymbol{O} & \boldsymbol{O} & \boldsymbol{O} & \boldsymbol{O} & \boldsymbol{O} & -\boldsymbol{I}_m & \boldsymbol{O} & \boldsymbol{O} & \boldsymbol{O} & \boldsymbol{I}_m
\end{bmatrix}.$$ (25)

Here $\boldsymbol{O}$ is null matrix, $\boldsymbol{I}_n$ and $\boldsymbol{I}_m$ are identity matrices of dimension n and m respectively, and $\boldsymbol{T}^{-1} = \boldsymbol{T}^T/2$. Finally, we have

$$\boldsymbol{f} = \boldsymbol{K}\boldsymbol{d},$$ (26)

where

$$\boldsymbol{K} = \boldsymbol{T}\text{diag}(\boldsymbol{K}^{00}, \boldsymbol{K}^{01}, \boldsymbol{K}^{10}, \boldsymbol{K}^{11})\boldsymbol{T}^{\mathrm{T}}/2.$$ (27)

If a boundary line node (either w or ϕ) is restrained, the corresponding rows and columns of the spectral stiffness matrix $\boldsymbol{K}$ are removed. In such a way, all possible BCs along the plate edges can be applied easily, leading to the final spectral stiffness matrix $\boldsymbol{K}_f$ for the plate subject to those BCs.

3. The Wittrick–Williams algorithm enhancement

A reliable and efficient solution technique to extract buckling load parameters from the analytical spectral stiffness matrix of a structure is the powerful Wittrick–Williams (WW) algorithm [65]. This algorithm ensures that no buckling load parameter is lost by monitoring the Sturm sequence of the ensuring matrix. According to the WW algorithm, the number of buckling eigenvalues between 0 and a trial buckling load coefficients (mode count J) of the final structure is

$$J = J_0 + s\{\boldsymbol{K}_f\},$$ (28)

where J_0 count is mode count of a plate element with all node lines fixed, and $s(\boldsymbol{K}_f)$ is the sign count (negative inertia) of $\boldsymbol{K}_f$ evaluated at the trial buckling load parameter. It is well known that in buckling analysis the first nonzero eigenvalue is of importance. However, J_0 is important in the method due to two reasons. First, for some of the most practical cases such as fully clamped cases, the J_0 is needed, otherwise, more elements should be involved in the modeling and will introduce unnecessary complexity. Second, higher buckling modes are sometimes very important in the optimization analysis especially in plate problems since mode veering is very likely to occur when changing certain parameters, in which the second (or higher) buckling mode will become the first. It is therefore important to trace the first couple of buckling modes in parametric or optimization analysis. However, the J_0 count is a difficult issue in the WW algorithm. In much previous research, J_0 count problems were avoided by partitioning a large element into a small mesh to ensure J_0 is zero, which affects the computational efficiency significantly. In this paper, an indirect method is applied to obtain J_0 by taking advantage of the closed-form buckling solutions of a fully guided plate. According to WW algorithm of Eq. (28), the mode count of a fully guided plate is given as $J_G = J_0 + s(\boldsymbol{K}_G)$, where $s(\boldsymbol{K}_G)$ is the sign count of the formulated stiffness matrix $\boldsymbol{K}_G$. Therefore, J_0 can be obtained from

$$J_0 = J_G - s(\boldsymbol{K}_G),$$ (29)

in which

$$s(\boldsymbol{K}_G) = \sum_{k,j \in \{0,1\}} s(\boldsymbol{K}_G^{kj}) = \sum_{k,j \in \{0,1\}} s(\boldsymbol{A}_{wv}^{kj})$$ (30)

It is noted that the above indirect strategy has been successfully applied to plate elements in [67,70] which improves the computational efficiency. However, when this strategy is applied to buckling analysis, the formulation of J_G will be completely different which will be described in what follows. In the case of all guided edges of the plate (*GGGG*), the shape function has the following relation

$$w(x, y) = C' \cos\left(\frac{m\pi}{2a}\check{x}\right) \cos\left(\frac{n\pi}{2b}\check{y}\right), \, m, n \in \{0, 1, 2, \ldots\} \text{ except for } m = n = 0 \tag{31}$$

where $\check{x} \in [0, 2a]$, $\check{y} \in [0, 2b]$. It should be noted that $m = n = 0$ is related to the situation when the plate remains flat which apparently has no physical meaning in the buckling analysis. Then, substituting Eq. (31) into Eq. (2) leads to the characteristic equation

$$m^4 + a_1 m^2 n^2 + a_2 n^4 + a_3 m^2 + a_4 n^2 + a_5 = 0, \tag{32}$$

where $a_1 = 2(a/b)^2$, $a_2 = (a/b)^4$, $a_3 = (2a/\pi)^2 N_x$, $a_4 = (2a/\pi)^2 (a/b)^2 N_y$, $a_5 = (2a/\pi)^4 k$. Next, we find the number of eigenvalues lower than the trial buckling load parameters which can be computed following the procedure below

Step 1 Initialise $J_G = 0$, input $[N_x, N_y]^T$;

Step 2 If $N_x \leq 0$ (zero or compressive)
- Let $n = 0$, Eq. (32) becomes $m^4 + a_3 m^2 = 0$, leading to $m^* = \sqrt{-a_3}$;
- Let m range from 0 to $\lfloor m^* \rfloor$, where $\lfloor m^* \rfloor$' is the largest integer not greater than m^*;
- Substituting m into Eq. (32) leads to $a_2 n^4 + b_2 n^2 + c_2 = 0$ where $b_2 = a_1 m^2 + a_4$, $c_2 = m^4 + a_3 m^2 - a_5$, resulting in a root $n^* = \sqrt{\left(-b_2 + \sqrt{b_2^2 - 4a_2 c_2}\right)/(2a_2)}$;
- $J_G = J_G + \lfloor n^* \rfloor$.

Step 3 Otherwise if $N_x > 0$ (tensile) and $N_y \leq 0$ (compressive)
- Let $m = 0$, Eq. (32) becomes $a_2 n^4 + a_4 n^2 = 0$, leading to $n^* = \sqrt{-a_4/a_2}$;
- Let n range from 0 to $\lfloor n^* \rfloor$;
- Substituting n into Eq. (32) leads to $m^4 + b_3 m^2 + c_3 = 0$ where $b_3 = a_1 n^2 + a_3$, $c_2 = a_2 n^4 + a_4 n^2 - a_5$, resulting in a root $m^* = \sqrt{\left(-b_3 + \sqrt{b_3^2 - 4c_3}\right)/2}$;
- $J_G = J_G + \lfloor m^* \rfloor$;

Step 4 Output the mode count J_G;

Step 5 Calculate $s(\boldsymbol{K}_G)$ and apply Eq. (29) leading to J_0;

Step 6 Calculate $\boldsymbol{K}_f$ and apply Eq. (28) resulting in the mode count J for the final structure; use the bisection method to find the critical buckling load parameter.

Buckling modes can be obtained by the following procedure. Firstly, arbitrary values are assigned to the selected degrees of freedom in the displacement vector, and then we can obtain the remaining values in the displacement vector $\boldsymbol{d}_f$. Then $\boldsymbol{d}^{kj}$ in Eq. (21) is determined by Eq. (24). Subsequently, unknown coefficients A_{1km}, A_{2km} and B_{1jn}, B_{2jn} are determined by Eq. (18), and the modal shapes are recovered by substituting unknowns into Eq. (11).

4. Results and discussions

The method described above is implemented into a MATLAB program which computes the critical buckling loads and mode shapes of rectangular plates with all possible BCs. The convergence, accuracy and numerical efficiency studies are carried out in Section 4.1 below. Then the method is applied to plates placed on Winkler foundation in Section 4.2 and plates with all possible boundary conditions in Section 4.3. Finally, Section 4.4 discusses the effect of inplane load combinations on the buckling characteristics.

Attention should be paid that in this section the letters âSâ âCâ âGâ and âFâ represent simply-supported, clamped, guided and free edges of the plate respectively. The compressive inplane stress in the *x*-direction is N_x, that in the *y*-direction is N_y. The dimensions of the plate in the *y* and *x* directions are always $2b \times 2a$ and the dimensionless critical buckling loads are defined accordingly when the results are presented.

4.1. Convergence, efficiency and numerical stability analysis

As shown in Table 2, the first six critical buckling load parameters of square plates subjected to compressive inplane stresses in both *x* and *y* directions ($N_x < 0$, $N_y < 0$) with four BCs (FFFF, CCSC, SCSC, CSCG) are tabulated. It is worth noting that the results calculated by the present method are performed with different numbers of modified Fourier series terms, where *N* and *M* are the numbers of terms in the *y* and *x* directions respectively. The global matrix size is proportional to the summation of *M* and *N* which is different from the commercial Finite Element (FE) package HyperWorks as well as other methods whose final matrix size is proportional to their products ($M \times N$) instead. All the results computed by the present method have the accuracy of 5 figure precision, which are compared with those obtained from the FEM software HyperWorks in Table 2. Among the four tabulated cases, it is obvious that the present method uses $5 + 5$ ($M + N$) terms

Table 2

First six critical buckling load parameters $\lambda = N_x(2a)^2/D\pi^2$ of square plates subjected to compressive inplane stresses in both x and y directions ($N_x = N_y < 0$) with different BCs.

$M = N$	Modes						Time (s)
FFFF	3	4	5	6	7	8	
2	**0.7391**	0.8152	1.2199	2.0079	2.0079	3.7081	0.22
5	**0.7391**	**0.8150**	**1.2196**	**2.0053**	**2.0053**	3.7059	0.28
10	**0.7391**	**0.8150**	**1.2196**	**2.0053**	**2.0053**	**3.7058**	0.38
20	**0.7391**	**0.8150**	**1.2196**	**2.0053**	**2.0053**	**3.7058**	0.77
30	**0.7391**	**0.8150**	**1.2196**	**2.0053**	**2.0053**	**3.7058**	1.59
FEM	0.7391	0.8150	1.2189	2.0053	2.0053	3.7063	167.00
CCSC	1	2	3	4	5	6	
2	4.3073	7.4184	8.8810	11.618	12.856	14.924	0.25
5	**4.3110**	7.4547	**8.8850**	**11.655**	**13.093**	16.017	0.29
10	**4.3110**	**7.4548**	**8.8850**	**11.655**	**13.093**	**16.018**	0.34
20	**4.3110**	**7.4548**	**8.8850**	**11.655**	**13.093**	**16.018**	0.54
30	**4.3110**	**7.4548**	**8.8850**	**11.655**	**13.093**	**16.018**	0.92
FEM	4.3126	7.4581	8.8873	11.654	13.103	16.026	184.00
SCSC	1	2	3	4	5	6	
2	3.8279	5.9088	8.6176	10.348	10.627	14.513	0.26
5	**3.8300**	**5.9243**	**8.6206**	**10.567**	**10.651**	14.923	0.28
10	**3.8300**	**5.9243**	**8.6206**	**10.567**	**10.651**	**14.924**	0.33
20	**3.8300**	**5.9243**	**8.6206**	**10.567**	**10.651**	**14.924**	0.59
30	**3.8300**	**5.9243**	**8.6206**	**10.567**	**10.651**	**14.924**	0.94
FEM	3.8314	5.9271	8.6228	10.575	10.648	14.922	179.00
CSCG	1	2	3	4	5	6	
2	**3.8248**	4.5179	7.9293	8.2736	9.3687	12.444	0.25
5	**3.8248**	**4.5219**	7.9579	**8.2738**	9.3744	**12.499**	0.30
10	**3.8248**	**4.5219**	**7.9580**	**8.2738**	**9.3745**	**12.499**	0.34
20	**3.8248**	**4.5219**	**7.9580**	**8.2738**	**9.3745**	**12.499**	0.59
30	**3.8248**	**4.5219**	**7.9580**	**8.2738**	**9.3745**	**12.499**	0.97
FEM	3.8234	4.5234	7.9634	8.2701	9.3716	12.497	171.00

to obtain six eigenvalues with four significant digits within less than 0.30 seconds, $10 + 10$ ($M + N$) terms leading to 5-bit precision results within 0.38 seconds. At the same time, the results are compared with finite element solutions computed by HyperWorks using a fine mesh (FEM, 300×300). The computation of both present method and FEM is performed on a PC equipped with a 3.3GHz Intel Core i5 processor and 4GB of memory. It can be seen from Table 2 that the present method takes less than 1% computation time of the FEM package HyperWorks in the four cases which meanwhile provides more accurate results than the FEM with only three significant digits.

4.2. Discussions on the effect of elastic Winkler foundation

After showing the computational performance of the proposed method, we now study the effects of elastic foundation on the buckling of plates. For square plates with four different boundary conditions (i.e., CCCC, FFFF, SSSS and GGGG) and subjected to compressive inplane stresses in the y-direction only ($N_x = 0$, $N_y < 0$), a total of 6 buckling eign-modes in terms of $\lambda = N_y(2a)^2/D\pi^2$ with respect to dimensionless foundation stiffnesses $k = \hat{k}/D$ (D is the bending stiffnesses and $\hat{k}$ is the stiffness of the Winkler foundation) are tabulated in Table 3. All results computed by the proposed method are provided with an accuracy of five significant figures. It can be found that the critical load parameters λ always show a monotonic and linear increase with the dimensionless foundation stiffness k for different boundary conditions and for different buckling modes, as shown in Fig. 2. More specifically, the linear relationship can be given by $\lambda_k = (1 + \epsilon k)\lambda_{k=0}$, where λ_k and $\lambda_{k=0}$ are the $\lambda's$ when dimensionless foundation stiffness is k and 0, respectively, and $\epsilon = (\lambda_k - \lambda_{k=0})/(k\lambda_{k=0})$ take different constants for different BCs and different eigen-modes as given in the last row of Table 3.

4.3. Buckling of rectangular plates subject to all possible boundary conditions

It can be found from Tables 4 and 5 that results computed by the present spectral stiffness method agrees very well with those of the symplectic superposition method [46,47] for three types of BCs (CCSS, CCCS, FFFF) and with three aspect ratios. It should be emphasized that the current spectral stiffness method utilizes a uniform formula but is capable of computing results for all possible BCs. This is in apparent contrast to the symplectic superposition method in [46,47], which needs to develop different formulations for each BCs.

Indeed, the effects of different BCs on the buckling of plates have been performed by many authors using different methods. But there has not been any meaningful research which provides the results published so far in the literature of all possible BCs for buckling analysis of square plates. To fill this gap, buckling results for a square plate with all 55

Table 3

Representative critical buckling load parameters $\lambda = N_y(2a)^2/D\pi^2$ of square plates under four different BCs and subjected to compressive inplane stresses in the y-direction only ($N_x = 0, N_y < 0$) with different dimensionless foundation stiffnesses $k = \hat{k}/D$.

k	λ					
	CCCC			FFFF	SSSS	GGGG
	λ_1	λ_3	λ_5	λ_1	λ_1	λ_1
0	10.074	19.465	26.374	0.922	4.000	1.000
0.1	10.074	19.465	26.374	0.9218	3.9998	1.0001
0.5	10.075	19.465	26.374	0.9220	4.0006	1.0004
1	10.075	19.466	26.374	0.9223	4.0012	1.0007
2	10.076	19.466	26.375	0.9229	4.0024	1.0014
3	10.077	19.467	26.376	0.9234	4.0036	1.0021
4	10.078	19.468	26.376	0.9240	4.0048	1.0028
5	10.079	19.469	26.377	0.9246	4.0060	1.0035
10	10.084	19.472	26.381	0.9274	4.0120	1.0070
100	10.177	19.536	26.452	0.9785	4.1199	1.0701
1000	11.094	20.175	27.158	1.4799	5.1994	1.7008
2000	12.095	20.898	27.934	2.0272	6.3989	2.4016
$\epsilon = \dfrac{\lambda_k - \lambda_{k=0}}{k\lambda_{k=0}}$	0.00010	0.00004	0.00003	0.00061	0.00030	0.00070
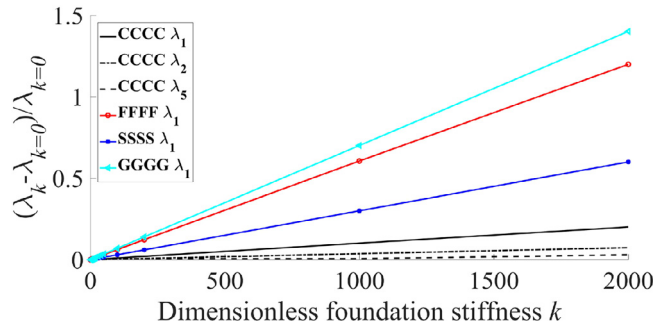
Fig. 2. Dependence of dimensionless foundation stiffness $k = \hat{k}/D$ on the critical buckling load parameters λ for four different boundary conditions.

Table 4

First seven critical buckling load parameters $\lambda = N_y(2a)^2/D\pi^2$ of square plates subjected to compressive inplane stresses in y directions only ($N_x = 0, N_y < 0$) with different aspect ratios and BCs.

BC	b/a	Methods	Modes						
			1	2	3	4	5	6	7
CCSS	0.5	Present	22.673	25.187	30.891	39.225	47.525	54.515	66.528
		Li et al. [47]	22.673	25.187	30.891	39.225	47.525	54.515	66.528
		FEM	22.674	25.189	30.895	39.233	47.536	54.532	66.560
	1	Present	6.2226	9.0222	14.596	19.618	22.414	22.803	28.879
		Li et al. [47]	6.2226	9.0222	14.596	19.618	22.414	22.803	28.879
		FEM	6.2228	9.0228	14.598	19.619	22.420	22.805	28.884
	1.5	Present	3.4386	7.1541	9.4458	11.639	13.077	16.606	18.680
		Li et al. [47]	3.4386	7.1541	9.4458	11.639	13.077	16.606	18.680
		FEM	3.4387	7.1551	9.4462	11.640	13.080	16.608	18.682
CCCS	0.5	Present	24.891	26.373	36.089	40.652	53.945	58.384	75.776
		Li et al.[47]	24.891	26.373	36.089	40.651	53.945	58.384	75.776
		FEM	24.892	26.376	36.095	40.660	53.960	58.408	75.820
	1	Present	8.0673	10.908	18.668	21.855	24.005	26.524	34.535
		Li et al. [47]	8.0673	10.908	18.668	21.855	24.005	26.524	34.535
		FEM	8.0675	10.909	18.672	21.856	24.008	26.532	34.544
	1.5	Present	5.3609	9.2515	11.418	13.005	17.054	20.819	20.973
		Li et al. [47]	5.3609	9.2515	11.418	13.005	17.054	20.819	20.973
		FEM	5.3613	9.2542	11.420	13.008	17.064	20.829	20.976

Table 5
First six critical buckling load parameters $\lambda = N_x(2a)^2/D$ of all edges free square plates subjected to compressive inplane stresses in both x and y directions ($N_x = N_y < 0$) with different aspect ratios.

b/a	Methods	Modes					
		3	4	5	6	7	8
0.5	Present	8.8812	12.194	33.983	37.511	39.251	55.169
	Li et al. [46]	8.8812	12.194	33.983	37.511	39.251	55.169
	FEM	8.8815	12.195	33.988	37.515	39.251	55.178
1	Present	7.2941	8.0437	12.036	19.791	19.791	36.575
	Li et al. [46]	7.2941	8.0437	12.036	19.791	19.791	36.575
	FEM	7.2944	8.0439	12.030	19.792	19.792	36.580
1.5	Present	3.8595	4.8417	10.090	12.990	13.133	19.076
	Li et al. [46]	3.8594	4.8417	10.090	12.990	13.133	19.076
	FEM	3.8595	4.8418	10.090	12.990	13.133	19.077

(a) CCCF   (b) FFFC
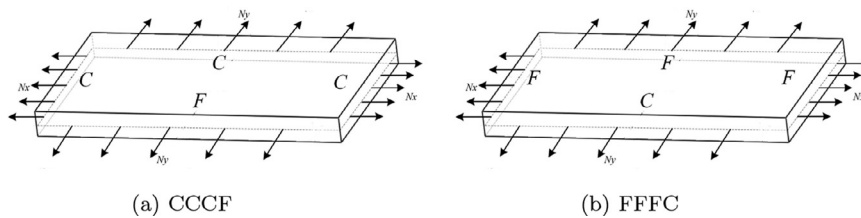
Fig. 3. Rectangular plates with two types of boundary conditions.

possible types of BCs without elastic foundation (dimensionless foundation stiffness $k = 0$) and compressed in both x and y directions, see Table 6. All results given in Table 6 have five significant figures (accurate up to the last figure quoted) which will serve as benchmark solutions.

4.4. Discussions on the effect of inplane load combinations

Fig. 3 shows the constraints of rectangular plates with two types of BCs in the x and y directions. Tables 7 and 8 shows the influences of load combination and aspect ratio on the critical buckling loads and mode shapes of rectangular plates with different BCs (FFFC, CCCF). It can be found that when the aspect ratio b/a and signs of both N_x and N_y (i.e., compressive or tensile) remain unchanged, the buckling load parameter under CCCF BC is always higher than that under FFFC BC. Under the two BCs, the increasing trend of buckling load parameters decreases gradually from the first mode to the seventh mode when the load combination remains unchanged and the aspect ratio b/a varies from 0.5 to 10. On the other hand, it can be found that when $b/a = 1$, the buckling load parameters for plates pressurive load only in the x-direction is higher than those for plates compressed only in the y-direction when subjected to FFFC BC. Similar observation can be made for plates under CCCF BC. It is within oneâs expectation that for rectangular plates, instabilities are much easier to occur along free edges than clamped edges.

Table 6

First six critical buckling load parameters $\lambda = N_y(2a)^2/D\pi^2$ of square plates without elastic foundation (dimensionless foundation stiffness $k = 0$) subjected to compressive inplane stresses in both x and y directions ($N_x = N_y < 0$) with 55 different types of BCs.

BC	Modes					
	1	2	3	4	5	6
SSSS	2.0000	5.0000	5.0000	8.0000	10.000	10.000
SSSC	2.6627	5.3648	6.6292	9.1533	10.239	12.620
SSSF	1.0554	2.1601	3.9702	5.0662	5.4172	8.3383
SCSC	3.8299	5.9242	8.6205	10.567	10.651	14.924
SCSF	1.1438	2.7654	4.0085	5.8359	6.7146	8.8462
SFSF	0.9322	1.1898	2.3151	3.8099	4.2204	5.1196
SSSG	1.2500	3.2500	4.2500	6.2500	7.2500	8.2500
SCSG	1.4811	4.3499	4.3937	6.9815	9.3120	9.3780
SGSF	0.9528	1.4482	3.3533	3.8705	4.5504	6.6546
SGSG	1.0000	2.0000	4.0000	5.0000	5.0000	8.0000
CCCC	5.3036	9.3337	9.3337	12.990	15.615	16.924
CCCS	4.3109	7.4548	8.8849	11.655	13.093	16.018
CCCF	2.8932	4.3271	7.4283	7.4540	8.8648	11.682
CSCF	2.8680	3.9077	5.8854	7.4282	8.6027	10.528
CFCF	2.7426	2.9714	4.0308	5.8406	7.3970	7.4597
CSCG	3.8247	4.5218	7.9578	8.2737	9.3744	12.499
CGCG	3.8299	4.0000	5.9242	8.1830	8.6205	10.567
CCCG	3.9234	5.5402	8.3377	9.9662	9.9993	13.961
CGCF	2.8291	3.9807	4.4814	7.4265	7.9257	8.2649
CGSG	2.0457	2.6627	5.3649	6.0468	6.6293	9.1534
SGGG	0.2500	1.2500	2.2500	3.2500	4.2500	6.2500
CGGG	1.0000	1.4811	4.0000	4.3499	4.3937	6.9815
SGFG	0.0000	1.0000	1.0551	2.1599	3.9700	4.0000
CGFG	0.2500	1.1436	2.2500	2.7652	4.0083	5.8357
GGFG	0.2500	0.9525	1.4480	2.2500	3.3531	3.8703
FGFG	0.0000	0.9322	1.0000	1.1899	2.3153	3.8099
GGGG	1.0000	1.0000	2.0000	4.0000	4.0000	5.0000
FFFF	0.0000	0.0000	0.7391	0.8150	1.2196	2.0053
CFSF	1.7870	1.9055	2.6985	5.2414	5.7159	5.8498
CCSS	3.2476	6.8169	7.0691	10.230	12.691	12.966
CCSF	1.8718	3.2222	5.7142	6.8066	7.3202	10.349
CSSF	1.8491	2.6696	5.3156	5.7588	6.7853	9.3026
SSFF	0.2037	0.9264	1.4201	2.8282	3.7871	4.3328
CSFF	0.4081	1.1064	2.1497	3.2377	4.2396	5.5373
CCFF	0.5783	1.3848	2.7502	3.6799	5.4711	6.5181
SFFF	0.0000	0.3089	0.8608	1.3974	1.6901	3.2951
CFFF	0.2396	0.4828	1.3035	2.1218	2.2863	3.8671
CSSG	2.1551	3.7309	6.1537	7.5399	7.6189	11.232
SSGG	0.5000	2.5000	2.5000	4.5000	6.5000	6.5000
CSGG	0.9575	2.6417	3.9579	5.4072	6.5767	8.9580
SSGF	0.2975	1.2799	2.2726	3.5560	4.2586	6.1537
SCGF	0.4586	2.1635	2.3284	4.0413	6.1810	6.2499
SGGF	0.2331	0.5788	2.1652	2.5175	2.7705	4.7490
SFGF	0.2300	0.3298	1.3768	2.1246	2.4845	3.8191
CCSG	2.3335	4.8020	6.2394	8.2740	9.6330	12.201
CCGF	0.7534	2.2912	3.6228	4.8796	6.3385	8.2040
CCGG	1.3259	3.9040	4.2309	6.2395	8.8483	9.1886
CGSF	1.8651	2.1465	3.7409	5.6430	6.2074	7.5270
CSGF	0.6856	1.4601	3.5621	4.3345	4.5079	7.0334
CGGF	0.7428	1.0076	2.6243	3.6372	4.0568	5.4921
CFGF	0.5405	0.9394	1.4554	3.4754	3.7395	4.3746
SGFF	0.0000	0.5013	0.9946	1.7727	2.4709	3.7616
CGFF	0.2440	0.6672	1.9415	2.2914	2.8923	4.4229
GGFF	0.1848	0.3049	1.1067	2.0608	2.2889	2.7368
GFFF	0.0000	0.2250	0.9502	0.9941	1.9134	2.4527

5. Conclusions

An analytical spectral stiffness method for buckling analysis of rectangular plates with general boundary conditions (BCs) has been proposed. This method integrates the merits of superposition method, stiffness-based method and the Wittrick–Williams algorithm. First, by introducing the modified Fourier series into the buckling governing differential equation (GDE), exact shape functions similar to the superposition method are derived, which guarantees the rapid convergence and high accuracy of the method. Then, applying symbolic calculation upon the exact shape functions leads to a spectral stiffness formulation, where any arbitrary BCs can be prescribed easily upon the unique stiffness-based formulation. This provides

Table 7

First seven critical buckling load parameters $\lambda = N_x(2a)^2/D\pi^2$ of plates with different aspect ratios and load combinations.

b/a	BC	Load combinations	Modes						
			1	2	3	4	5	6	7
0.5	FFFC	$N_x = 0, N_y < 0$	0.9800	2.4657	8.3157	9.0424	10.351	19.342	19.681
		$N_x < 0, N_y = 0$	3.3282	3.7035	6.4928	10.8151	17.482	23.633	24.001
		$N_x = N_y < 0$	0.9766	1.6328	2.6689	4.4258	7.7661	8.5993	9.1661
	CCCF	$N_x = 0, N_y < 0$	4.2268	12.567	14.244	25.337	27.666	34.561	42.588
		$N_x < 0, N_y = 0$	7.6996	10.607	18.231	25.971	37.638	41.653	42.541
		$N_x = N_y < 0$	3.0137	7.4873	9.1652	12.889	14.491	19.519	22.857
1	FFFC	$N_x = 0, N_y < 0$	0.2406	1.8240	2.1583	3.8087	6.0684	7.7350	8.3553
		$N_x < 0, N_y = 0$	0.6123	1.3961	4.2734	5.7179	6.3675	9.2710	11.605
		$N_x = N_y < 0$	0.2397	0.4828	1.3035	2.1218	2.2864	3.8670	4.2838
	CCCF	$N_x = 0, N_y < 0$	3.9091	9.7102	12.252	13.791	21.014	24.460	24.809
		$N_x < 0, N_y = 0$	4.5761	8.5996	12.628	14.057	16.350	21.765	24.428
		$N_x = N_y < 0$	2.8929	4.3272	7.4274	7.4540	8.8648	11.682	12.979
3	FFFC	$N_x = 0, N_y < 0$	0.2363	0.6586	1.3027	1.6803	1.9177	2.1691	2.3450
		$N_x < 0, N_y = 0$	0.4562	0.9705	1.3399	1.4504	2.1221	3.2156	3.4046
		$N_x = N_y < 0$	0.2336	0.3739	0.6381	0.9071	1.0248	1.2660	1.3808
	CCCF	$N_x = 0, N_y < 0$	3.8743	7.3553	7.4754	8.4133	9.1306	10.580	11.153
		$N_x < 0, N_y = 0$	4.0252	4.5544	5.8137	8.1803	8.2153	8.6671	9.6764
		$N_x = N_y < 0$	2.8465	3.8490	3.9076	4.0125	4.4370	5.2522	6.3767
10	FFFC	$N_x = 0, N_y < 0$	0.1172	0.1900	0.2840	0.3975	0.5312	0.6848	0.8586
		$N_x < 0, N_y = 0$	0.1915	0.3279	0.5107	0.7471	0.9394	0.9908	1.0374
		$N_x = N_y < 0$	0.1164	0.1737	0.1881	0.2801	0.2808	0.3908	0.4092
	CCCF	$N_x = 0, N_y < 0$	3.8729	7.0084	7.0133	7.1201	7.1372	7.3130	7.3369
		$N_x < 0, N_y = 0$	3.9893	4.0373	4.1215	4.2525	4.4356	4.6777	4.9876
		$N_x = N_y < 0$	2.8446	3.7690	3.7695	3.8016	3.8035	3.8491	3.8588

the convenience of the applications of general boundary conditions, which is superior to the superposition method where different building blocks are required for different BCs. Finally, the Wittrick–Williams algorithm has been applied as the solution technique with the most important issue J_0 count resolved, which endows the method high efficiency, robustness and certainty that no mode is missed. It has been demonstrated that the present method provides highly accurate solutions in an extremely efficient manner, by taking less than one per cent of the time required by the commercial finite element packages. Besides, this paper provides critical buckling load parameters for rectangular plates subjected to all possible BCs as benchmark solutions. Finally, the effects of foundation stiffness, load combinations, and aspect ratio on the buckling behaviors are investigated. The present method has provided a uniform analytical formulation for plate buckling analysis with general BCs and foundation supports, and meanwhile provide valuable references for future research in this field.

Acknowledgments

References

[1] M. Komur, M. Sonmez, Elastic buckling behavior of rectangular plates with holes subjected to partial edge loading, J. Constr. Steel Res. 112 (2015) 54–60, doi:10.1016/j.jcsr.2015.04.020.

[2] M. Ravari, S. Talebi, A. Shahidi, Analysis of the buckling of rectangular nanoplates by use of finite-difference method, Meccanica 49 (6) (2014) 1443–1455, doi:10.1007/s11012-014-9917-x.

[3] D. Rui, D. Fang-yun, Z. Ying, Boundary element method for buckling eigenvalue problem and its convergence analysis, Appl. Math. Mech. 23 (2) (2002) 155–168, doi:10.1007/BF02436557.

[4] D.J. Dawe, V. Peshkam, Buckling and vibration of finite-length composite prismatic plate structures with diaphragm ends, part I: finite strip formulation, Comput Methods Appl. Mech. Eng. 77 (1–2) (1989) 1–30, doi:10.1016/0045-7825(89)90126-6.

[5] M. Huang, D. Thambiratnam, Analysis of plate resting on elastic supports and elastic foundation by finite strip method, Comput. Struct. 79 (29–30) (2001) 2547–2557, doi:10.1016/S0045-7949(01)00134-1.

[6] X. Wang, X. Wang, X. Shi, Accurate buckling loads of thin rectangular plates under parabolic edge compressions by the differential quadrature method, Int. J. Mech. Sci. 49 (4) (2007) 447–453, doi:10.1016/j.ijmecsci.2006.09.004.

[7] Ö. Civalek, Application of differential quadrature (DQ) and harmonic differential quadrature (HDQ) for buckling analysis of thin isotropic plates and elastic columns, Eng. Struct. 26 (2) (2004) 171–186, doi:10.1016/j.engstruct.2003.09.005.

[8] A.A. Jafari, S.A. Eftekhari, An efficient mixed methodology for free vibration and buckling analysis of orthotropic rectangular plates, Appl. Math. Comput. 218 (6) (2011) 2670–2692, doi:10.1016/j.amc.2011.08.008.

[9] Ö. Civalek, A. Korkmaz, Ç. Demir, Discrete singular convolution approach for buckling analysis of rectangular kirchhoff plates subjected to compressive loads on two-opposite edges, Adv. Eng. Softw. 41 (4) (2010) 557–560, doi:10.1016/j.advengsoft.2009.11.002.

Table 8

First three buckling modes of plates with different aspect ratios and load combinations.
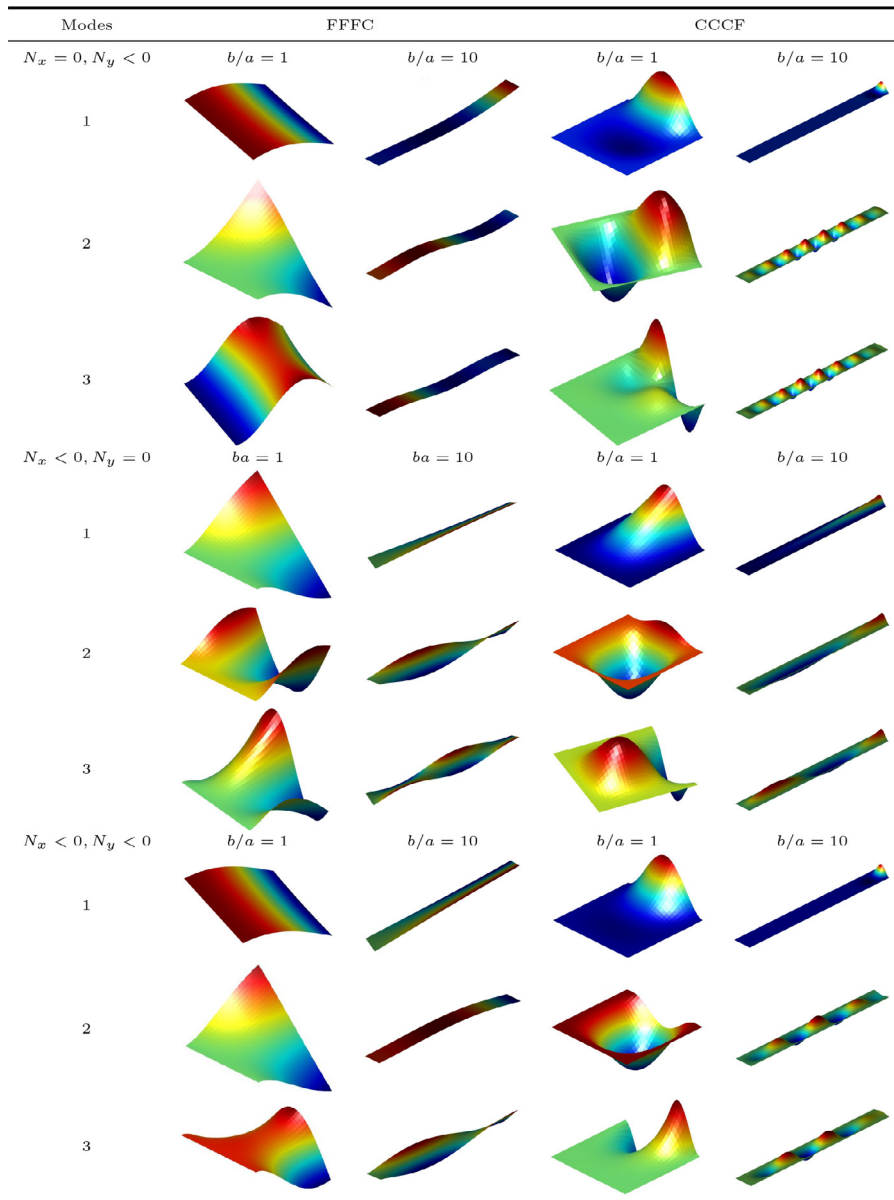
[10] S. Ullah, Y. Zhong, J. Zhang, Analytical buckling solutions of rectangular thin plates by straightforward generalized integral transform method, Int. J. Mech. Sci. 152 (January) (2019) 535–544, doi:10.1016/j.ijmecsci.2019.01.025.

[11] D. Brush, B. Almroth, Buckling of Bars, Plates and Shells, 1975.

[12] A.W. Leissa, Buckling of Laminated Composite Plates and Shell Panels, Technical Report, US government, 1985.

[13] J. Reddy, Mechanics of Laminated Composite Plates and Shells Theory and Analysis, 2nd ed., CRC Press, 2003.

[14] G.H. Bryan, On the stability of a plane plate under thrusts in its own plane, with applications to the buckling of the sides of a ship, Proc. Lond. Math. Soc. 22 (1) (1890) 54–67.

[15] M. Stein, J. Neff, Buckling Stresses of Simply Supported Rectangular Flat Plates in Shear, 1222, National Advisory Committee for Aeronautics, 1947, doi:10.1016/s0016-0032(31)91049-1.

[16] W. Wittrick, Correlation between some stability problems for orthotropic and isotropic plates under bi-axial and uni-axial direct stress, Aeronaut. Q. 4 (01) (1951) 83–92, doi:10.1017/s0001925900000809.

[17] C. Libove, Buckle pattern of biaxially compressed simply supported orthotropic rectangular plates, J. Compos. Mater. 17 (1) (1983) 45–48, doi:10.1177/002199838301700104.

[18] J.H. Kang, A.W. Leissa, Vibration and buckling of SS-F-SS-F rectangular plates loaded by in-plane moments, Int. J. Struct. Stab. Dyn. 01 (04) (2001) 527–543, doi:10.1142/s0219455401000299.

[19] Z.Y. Huang, C.F. Lü, W.Q. Chen, Benchmark solutions for functionally graded thick plates resting on Winkler-Pasternak elastic foundations, Compos. Struct. 85 (2) (2008) 95–104, doi:10.1016/j.compstruct.2007.10.010.

[20] C.R. Briscoe, S.C. Mantell, J.H. Davidson, Buckling of a plate on a pasternak foundation under uniform in-plane bending loads, Int. J. Struct. Stab. Dyn. 13 (3) (2013) 1–12, doi:10.1142/S0219455412500708.
[21] A.W. Leissa, J.H. Kang, Exact solutions for vibration and buckling of an SS-C-SS-C rectangular plate loaded by linearly varying in-plane stresses, Int. J. Mech. Sci. 44 (9) (2002) 1925–1945, doi:10.1016/S0020-7403(02)00069-3.
[22] J.H. Kang, A.W. Leissa, Exact solutions for the buckling of rectangular plates having linearly varying in-plane loading on two opposite simply supported edges, Int J Solids Struct 42 (14) (2005) 4220–4238, doi:10.1016/j.ijsolstr.2004.12.011.
[23] H. Zhong, C. Gu, Buckling of symmetrical cross-ply composite rectangular plates under a linearly varying in-plane load, Compos. Struct. 80 (1) (2007) 42–48, doi:10.1016/j.compstruct.2006.02.030.
[24] M. Bodaghi, A. Saidi, Stability analysis of functionally graded rectangular plates under nonlinearly varying in-plane loading resting on elastic foundation, Arch. Appl. Mech. 81 (6) (2011) 765–780, doi:10.1007/s00419-010-0449-0.
[25] M. Saeidifar, S. Sadeghi, M. Saviz, Analytical solution for the buckling of rectangular plates under uni-axial compression with variable thickness and elasticity modulus in the y-direction, Proc. Inst. Mech. Eng. Part C: J. Mech. Eng. Sci. 224 (1) (2010) 33–41, doi:10.1243/09544062JMES1562.
[26] E. Ruocco, V. Mallardo, Buckling analysis of levy-type orthotropic stiffened plate and shell based on different strain-displacement models, Int. J. Non-Linear Mech. 50 (2013) 40–47, doi:10.1016/j.ijnonlinmec.2012.11.007.
[27] P. Seide, Compressive buckling of a long simply supported plate on an elastic foundation, J. Aerosp. Sci. 25 (6) (1958) 382–384, doi:10.2514/8.7691.
[28] K.Y. Lam, C.M. Wang, X.Q. He, Canonical exact solutions for levy-plates on two-parameter foundation using Green's functions, Eng. Struct. 22 (4) (2000) 364–378, doi:10.1016/S0141-0296(98)00116-3.
[29] L.H. Yu, C.Y. Wang, Buckling of rectangular plates on an elastic foundation using the levy method, AIAA J. 46 (12) (2008) 3163–3166, doi:10.2514/1.37166.
[30] A. Jahanpour, F. Roozbahani, An applicable formula for elastic buckling of rectangular plates under biaxial and shear loads, Aerosp. Sci. Technol. 56 (2016) 100–111, doi:10.1016/j.ast.2016.07.005.
[31] H. Akhavan, S. Hosseini Hashemi, H.R. Damavandi Taher, A. Alibeigloo, S. Vahabi, Exact solutions for rectangular mindlin plates under in-plane loads resting on pasternak elastic foundation. part i: buckling analysis, Comput. Mater. Sci. 44 (3) (2009) 968–978, doi:10.1016/j.commatsci.2008.07.004.
[32] A. Moslemi, B. Neya, J. Amiri, Benchmark solution for buckling of thick rectangular transversely isotropic plates under biaxial load, Int. J. Mech. Sci. 131–132 (2017) 356–367, doi:10.1016/j.ijmecsci.2017.07.006.
[33] M. Bodaghi, A.R. Saidi, Levy-type solution for buckling analysis of thick functionally graded rectangular plates based on the higher-order shear deformation plate theory, Appl. Math. Model. 34 (11) (2010) 3659–3673, doi:10.1016/j.apm.2010.03.016.
[34] H.T. Thai, S.E. Kim, Closed-form solution for buckling analysis of thick functionally graded plates on elastic foundation, Int. J. Mech. Sci. 75 (2013) 34–44, doi:10.1016/j.ijmecsci.2013.06.007.
[35] W. Wittrick, F. Williams, Buckling and vibration of anisotropic or isotropic plate assemblies under combined loadings, Int. J. Mech. Sci. 16 (4) (1974) 209–239, doi:10.1016/0020-7403(74)90069-1.
[36] D. McGowan, Development of Curved-plate Elements for the Exact buckling Analysis of Composite Plate Assemblies Including Transverse-shear Effects, Ph.D. thesis, Old Dominion University, 1997.
[37] M. Damghani, D. Kennedy, C. Featherston, Critical buckling of delaminated composite plates using exact stiffness analysis, Comput. Struct. 89 (13–14) (2011) 1286–1294, doi:10.1016/j.compstruc.2011.04.003.
[38] M. Damghani, D. Kennedy, C. Featherston, Global buckling of composite plates containing rectangular delaminations using exact stiffness analysis and smearing method, Comput. Struct. 134 (2014) 32–47, doi:10.1016/j.compstruc.2013.12.005.
[39] F.A. Fazzolari, J. Banerjee, M. Boscolo, Buckling of composite plate assemblies using higher order shear deformation theory: an exact method of solution, Thin-Walled Struct. 71 (2013) 18–34, doi:10.1016/j.tws.2013.04.017.
[40] S. Ilanko, L.E. Monterrubio, Y. Mochida, The Rayleigh–Ritz Method for Structural Analysis, John Wiley & Sons, 2014, doi:10.1002/9781118984444.
[41] L.E. Monterrubio, Frequency and buckling parameters of box-type structures using the Rayleigh-Ritz method and penalty parameters, Comput. Struct. 104–105 (2012) 44–49, doi:10.1016/j.compstruc.2012.03.010.
[42] D. Gorman, Vibration Analysis of Plates by the Superposition Method, World Scientific, London, 1999.
[43] D. Gorman, Free vibration and buckling of in-plane loaded plates with rotational elastic edge support, J. Sound Vib. 229 (4) (2000) 755–773, doi:10.1006/jsvi.1999.2527.
[44] W.L. Cleghorn, S.D. Yu, Analysis of buckling of rectangular plates using the method of superposition, Trans. Can. Soc. Mech. Eng. 16 (2) (1992) 185–199.
[45] S. Papkov, J.R. Banerjee, A new method for free vibration and buckling analysis of rectangular orthotropic plates, J. Sound Vib. 339 (2015) 342–358, doi:10.1016/j.jsv.2014.11.007.
[46] R. Li, X. Zheng, H. Wang, S. Xiong, K. Yan, P. Li, New analytic buckling solutions of rectangular thin plates with all edges free, Int. J. Mech. Sci. 144 (April) (2018) 67–73, doi:10.1016/j.ijmecsci.2018.05.041.
[47] B. Wang, P. Li, R. Li, Symplectic superposition method for new analytic buckling solutions of rectangular thin plates, Int. J. Mech. Sci. 119 (November) (2016) 432–441, doi:10.1016/j.ijmecsci.2016.11.006.
[48] R. Li, H. Wang, X. Zheng, S. Xiong, Z. Hu, X. Yan, Z. Xiao, H. Xu, P. Li, New analytic buckling solutions of rectangular thin plates with two free adjacent edges by the symplectic superposition method, Eur. J. Mech.: A/Solids 76 (May 2018) (2019) 247–262, doi:10.1016/j.euromechsol.2019.04.014.
[49] J. Tenenbaum, A. Deutsch, M. Eisenberger, Analytical buckling loads for rectangular orthotropic and symmetrically laminated plates, AIAA J. (2019) 1–11, doi:10.2514/1.j058536.
[50] J. Tenenbaum, A. Deutsch, M. Eisenberger, Analytical buckling loads for corner supported rectangular orthotropic and symmetrically laminated plates, Z. Angew. Math. Mech. (2019) 1–20, doi:10.1002/zamm.201900142.
[51] I. Shufrin, M. Eisenberger, Stability and vibration of shear deformable plates - first order and higher order analyses, Int. J. Solids Struct. 42 (3–4) (2005) 1225–1251, doi:10.1016/j.ijsolstr.2004.06.067.
[52] I. Shufrin, O. Rabinovitch, M. Eisenberger, Buckling of symmetrically laminated rectangular plates with general boundary conditions – a semi analytical approach, Compos Struct 82 (4) (2008) 521–531, doi:10.1016/j.compstruct.2007.02.003.
[53] A. Lopatin, E. Morozov, Approximate buckling analysis of the CCFF orthotropic plates subjected to in-plane bending, Int. J. Mech. Sci. 85 (2014) 38–44, doi:10.1016/j.ijmecsci.2014.05.003.
[54] E. Ruocco, V. Minutolo, S. Ciaramella, A generalized analytical approach for the buckling analysis of thin rectangular plates with arbitrary boundary conditions, Int. J. Struct. Stab. Dyn. 11 (01) (2011) 1–21, doi:10.1142/S0219455411003963.
[55] E. Ruocco, V. Minutolo, Buckling of composite plates with arbitrary boundary conditions by a semi-analytical approach, Int. J. Struct. Stab. Dyn. 12 (05) (2012) 1250033, doi:10.1142/s0219455412500332.
[56] E. Ruocco, M. Fraldi, An analytical model for the buckling of plates under mixed boundary conditions, Eng. Struct. 38 (2012) 78–88, doi:10.1016/j.engstruct.2011.12.049.
[57] S. Ilanko, Penalty methods for finding eigenvalues of continuous systems: emerging challenges and opportunities, Comput. Struct. 104–105 (2012) 50–54, doi:10.1016/j.compstruc.2012.02.017.
[58] S. Ilanko, D. Kennedy, B. Topping, Special issue: eigenvalues of continuous systems, Comput. Struct. 3 (2012) 104–105, doi:10.1016/j.compstruc.2012.05.006.
[59] A.D. Kerr, An extended Kantorovich method for the solution of eigenvalue problems, Int. J. Solids Struct. 5 (1969) 559–572, doi:10.1016/0020-7683(69)90028-6.
[60] X. Liu, J.R. Banerjee, Free vibration analysis for plates with arbitrary boundary conditions using a novel spectral-dynamic stiffness method, Comput. Struct. 164 (2016) 108–126, doi:10.1016/j.compstruc.2015.11.005.

[61] L. Monterrubio, S. Ilanko, Proof of convergence for a set of admissible functions for the Rayleigh–Ritz analysis of beams and plates and shells of rectangular planform, Comput. Struct. 147 (2015) 236–243, doi:10.1016/j.compstruc.2014.09.008.
[62] X. Liu, J. Banerjee, An exact spectral-dynamic stiffness method for free flexural vibration analysis of orthotropic composite plate assemblies – Part I: theory, Compos. Struct. 132 (2015) 1274–1287, doi:10.1016/j.compstruct.2015.07.020.
[63] X. Liu, J.R. Banerjee, An exact spectral-dynamic stiffness method for free flexural vibration analysis of orthotropic composite plate assemblies – Part II: applications, Compos. Struct. 132 (2015) 1288–1302, doi:10.1016/j.compstruct.2015.07.022.
[64] X. Liu, H.I. Kassem, J. Banerjee, An exact spectral dynamic stiffness theory for composite plate-like structures with arbitrary non-uniform elastic supports, mass attachments and coupling constraints, Compos. Struct. 142 (2016) 140–154, doi:10.1016/j.compstruct.2016.01.074.
[65] W. Wittrick, F. Williams, A general algorithm for computing natural conditions conditions of elastic structures, Q. J. Mech. Appl. Math. 24 (3) (1971) 263–284.
[66] X. Liu, On Some Eigenvalue Problems for Elastic Instabilities in Tension, University of Glasgow, 2013 Ph.D. thesis.
[67] X. Liu, Spectral dynamic stiffness formulation for inplane modal analysis of composite plate assemblies and prismatic solids with arbitrary classical/nonclassical boundary conditions, Compos. Struct. 158 (2016) 262–280, doi:10.1016/j.compstruct.2016.09.019.
[68] Y. Frostig, G.J. Simitses, Buckling of ring-stiffened multi-annular plates, Comput. Struct. 29 (3) (1988) 519–526.
[69] C.D. Coman, X. Liu, Buckling-resistant thin annular plates in tension, Math. Mech. Solids 19 (8) (2014) 925–951, doi:10.1177/1081286513493108.
[70] X. Liu, J. Banerjee, A spectral dynamic stiffness method for free vibration analysis of plane elastodynamic problems, Mech. Syst. Signal Process. 87 (2017) 136–160, doi:10.1016/j.ymss.2016.10.017.